

Quantum Hall effect: from the drude conductivity model to the Chern-Simons field description

G. B. de Gracia^{*1}, B.M. Pimentel²

¹Universidade Federal do ABC, Centro de Matemática, 09210-580, Santo André, SP, Brasil.

²Universidade Estadual Paulista, Instituto de Física Teórica, 01156-970, São Paulo, SP, Brasil.

Received on February 18, 2023. Revised on April 15, 2023. Accepted on May 11, 2023.

The goal of this article is to introduce the quantum Hall effect (QHE) from its classical roots to the quantum integer and fractional versions. This is a robust phenomenon with topological nature. Regarding the fractional quantum Hall effect, its phenomenology and the possibility of vortices with fractional charges are also discussed. The lattice structure of graphene, one of the possible planar matter samples in which quantum Hall effects can occur, is also analyzed. The calculation of the Landau levels occurring in this specific substrate is carefully performed. For completeness, a field description for a whole class of these systems, the ones related to the fractional quantum Hall effect, is also reviewed.

Keywords: Transport properties, Hall effect, topological.

1. Introduction

The Hall effect [1] and its microscopic quantum description (QHE) are associated to a wide variety of condensed matter phenomena with a well-established experimental [2, 3] and theoretical basis [4–6]. Roughly speaking, it is related to the emergence of a quantized transverse conductivity in a class of materials possessing a high scattering time between the charge carriers and the material lattice, such that their transport properties approximately depend just on the intense external magnetic field of typical order $\sim (1 - 50)$ Tesla. The samples are two-dimensional layers of semiconductors appearing in wells associated to GaAs or the MOSFET (Metal-Oxide-Semiconductor Field Effect Transistor.) transistors, for example. The phenomenon is generally observed at very low temperatures (originally verified at $T < 0,5$ K) and high external magnetic field [6] in order to avoid temperature fluctuation noise. However, there are more recent achievements associated with its realization at higher temperatures, even in the room one [7].

The basic setup of the classical Hall effect consists of a perpendicular external magnetic field applied over a planar matter sample. If an electric field is established in some direction parallel to the plane, the Lorentz force tends to bend the trajectory of the charge carriers, leading to a non-zero perpendicular conductivity. In 1879, E.H. Hall was the first to present a systematic investigation on this phenomenon, obtaining a linear relation between the applied magnetic field and the resistance associated to the transverse current [1]. Since it depends

on the charge and density of the mobile carriers, it became a useful experimental tool to investigate a wide set of matter samples in laboratory. However, just in the 50's it became widely used in the industry [8].

Classical Hall devices are often used to detect magnetic fields, but also play the key role in several sensors to detect pressure and temperature, for example. These devices are present in computers, automobiles, aircraft and in medical technology [9].

There are recent works associated to the development of pedagogical experimental activities involving Hall phenomenology. It is interesting to mention the proposal based on experiments with bismuth samples specially designed for the realization of the classical Hall effect in middle school laboratories [10]. There is also a guide for an undergraduate Hall effect experiment in copper [11] and a correlated idea associated to magnetic polarity and Hall sensors [12]. In [13], the Hall effect is applied as a tool to describe the microscopic structure of a wire as well as its charge density from a set of macroscopic measurements.

The quantum nature of this phenomenon was unveiled in the eighties. Basically, a more accurate analysis of the experimental data on the Hall resistivity graph revealed plateaus at quantized values. The underlying physics is beyond the simple Lorentz force approximation, depending on purely quantum and topological properties.

Regarding the structure of this present article, it is focused on the quantum aspects of the Hall effect. A brief review on the classical Hall effect is provided in order to define a conceptual basis for a self-contained introduction on the discussion of the quantum aspects. The articles and books mentioned in the previous paragraphs can also contribute to gain valuable insights in

*Correspondence email address: gb9950@gmail.com

the classical phenomenology. Regarding the quantum content, the harmonic oscillator structure is considered to introduce the integer quantum Hall effect in a suitable manner for undergraduate students. After that, more subtle concepts are introduced step by step, as well as its phenomenological motivations. Then, while covering the key discussions on the subject, we carefully introduce all the necessary correlated tools, contributing to improve the reader's formation.

The integer quantum Hall effect was discovered in 1980 by von Klitzing [3]. It occurs in two-dimensional electron gases, exhibiting well-defined plateaus at quantized Hall conductivities associated to multiples of e^2/h . By applying a gate voltage on the Si-MOSFET transistor, he obtained a nearly 2D electron gas. As the bottom of the conduction band is pushed down from the Fermi energy, electrons accumulate in a triangular potential well near the Si/SiO_2 interface on a small width of ≈ 50 Angstroms.

In 1982, F. Tsui et al., observed the fractional quantum Hall effect in samples with high mobility such as $GaAs/AlGaAs$ [3]. The fractional values for the conductivity are associated to the electron-electron interaction. The nearly planar electron gas formed in this structure has a bigger width of ≈ 100 Angstroms [14].

Then, a natural non-relativistic description for the integer case is given by the Landau model, leading to gaped energy levels. The fractional case, associated to a class of fractional values for conductance, is described by the so-called Laughlin wave function [15].

Regarding the Chern-Simons model, it can be related to (QHE) by means of the seminal work of [16] which is based on a unitary transformation that relates the Hamiltonian describing polarized¹ fermions interacting with an external electromagnetic field to a system of bosons interacting with external photons and also with a new quantum field responsible for changing the statistical nature of the charge carriers. This transformation exists just for some Lagrangian parameter values that lead exactly to a class of observed fractional conductivity values. This model also predicts the existence of fractionally charged vortices. It is worth to mention that the Chern-Simons term also arises in another field theory context. If one couple an external electromagnetic field to fermions in its two-dimensional representation and integrate them out, the obtained low energy effective action contains this aforementioned term [5].

We also give a brief review on the description of the specific properties of the material samples in which the (QHE) occurs. The description of the lattice structure of graphene [17] with its emerging low energy quasi-particle excitations is an interesting content to be analyzed here. It is one representative of a class of two band

Hamiltonians in condensed matter with applications from (QHE) to topological insulators, see [18, 19]. These books have several examples of a variety of quasi-particles in different condensed matter phenomena. The monolayer graphene case is characterized by two independent low energy modes, the so-called valleys [20]. The control of their properties is related to the recent field of valleytronics [21] with important applications in technology. Robust topological quantum states, such as the ones associated with (QHE) can be employed to store information suitable to be applied in quantum computing [18].

The paper is organized as follows. The second section is devoted to the experimental description of the classical Hall effect. In the section 3, we use the Drude conductivity model to describe very clean samples and then infer the emergence of a transverse conductivity for a system under an external magnetic field. Throughout the section 4, we introduce the integer quantum Hall effect (IQHE) phenomenology and a proposal to describe it by means of a well established quantization procedure. In the section 5 we obtain, from the previous developments, the quantized values for the conductivity. In the section 6, we discuss the importance of a small amount of impurity in order to provide accessible bulk states associated to the formation of plateaus in Hall resistivity. It is a suitable point to comment about the topological nature of the quantum Hall effect. The section 7 introduces the fractional quantum Hall effect (FQHE) and correlated issues. In section 8, the lattice structure of a specific sample, the graphene layer, is analyzed and the emerging low energy description is obtained. In the section 9, an interesting field description for the fractional quantum Hall effect based on the statistical changing is reviewed. Finally, in section 10, we conclude and present new perspectives. The S.I. units are used throughout.

2. Experimental Origin of the Classical Hall Effect

The classical Hall effect was discovered in 1879 by Edwin H. Hall [1]. The Maxwell's Treatise on Electricity and Magnetism, claimed that the effect of a magnetic field on a fixed conductor is just to create a fast transient induction current due to the variation of magnetic flux associated with turning on this external field. Contrary to this claim, Hall showed that by applying an electric field to this system a transverse current arises with the resistance to its establishment being expressed as

$$R_H = \frac{B}{nq} \quad (1)$$

with B denoting the magnetic field, n being the charge carrier density and q representing its charge.

It is interesting to mention that this effect can be used as a method to infer the charge or the density of

¹ Electrons with their spins aligned in order to minimize the Zeeman effect. Different from this latter case, the Hall effect quantum is associated to the quasi-particle effective mass. It implies that it is much higher than the Zeeman effect quantum.

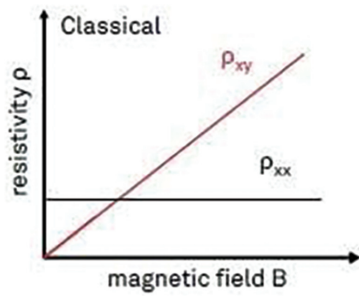


Figure 1: Transverse and longitudinal resistivity dependence on the external magnetic field. The transverse resistivity linearly increases with the magnetic field. At microscopic level, it displays a quantized plateau structure [22]. The longitudinal one is independent of this field.

the charged particles in a given sample. The qualitative dependence of the Hall resistivity with the increase of a magnetic field is given in Figure 1.

The Hall effect is an important phenomenon, being relevant in the metrology area. Also, after 70 years from its discovery, it began to be more often applied on the industry. Hall effect devices can detect the proximity of a magnetic field due to the emergence of the transverse conductivity. It can be applied, as magnetic sensors in automotive systems, as proximity sensors and transducers [23], for example.

3. The Theoretical Description Using the Drude Model

In order to provide a realistic description, the properties of the medium in which the charged particle propagates must be taken into account. Adding to the Lorentz force, a term representing the effect of the material medium on the charge carriers yields the equation of motion

$$m \frac{d\vec{V}}{dt} = -e\vec{E} - e\vec{V} \times \vec{B} - m \frac{\vec{V}}{\tau} \tag{2}$$

with the τ denoting the average time between two successive charge collisions with the material medium. For example, a conductor like copper has $\tau \sim 10^{-19} s$. The variable m denotes the effective mass of the charge carriers associated to the microscopic physics. This modified Lorentz force equation defines the so-called Drude model. Here, it is considered the particular case of an applied magnetic field perpendicular to the plane of the sample. It is worth to mention the reference [24], in which a complete and comprehensive review of the Drude model is developed. The equilibrium solution (steady current)

$$\frac{d\vec{V}}{dt} = 0 \tag{3}$$

furnishes a relation between the applied electric field and the associated current density

$$J_i = \sigma_{ij} E_j, \quad \sigma = \frac{ne^2\tau}{m(1 + \omega_B^2\tau^2)} \begin{pmatrix} 1 & -\omega_B\tau \\ \omega_B\tau & 1 \end{pmatrix} \tag{4}$$

in which $\omega_B = \frac{eB}{m}$ denotes the cyclotron frequency due to the interaction with the magnetic field. The current density is defined as $J_i = -neV_i$.

The resistivity matrix ρ reads

$$\rho = \frac{m}{ne^2\tau} \begin{pmatrix} 1 & \omega_B\tau \\ -\omega_B\tau & 1 \end{pmatrix} \tag{5}$$

It means that the transverse conducting properties are independent of the material medium properties, leading to the well known universality and robustness of Hall phenomena. Namely, this explains why the effect is observed in a wide variety of materials. As we are going to see, the quantum version of this phenomenon is topologically protected. It implies that the transport properties are resistant to small perturbation of the system's parameters.

Then, considering the limit $\tau \rightarrow \infty$ (much bigger than the scattering time of conducting materials, leading to low influence from the medium.) one gets $\sigma_{xx} \rightarrow 0$, $\rho_{xx} \rightarrow 0$ and

$$\rho_{xy} = \frac{m\omega_B}{ne^2} = \frac{B}{ne} \tag{6}$$

This is the prototype of the samples in which the Hall effect occur. For example, for an insulator like silica glass, $\tau \sim 10^3 s$ various orders bigger than in copper case. That is the physical meaning of taking the limit $\tau \rightarrow \infty$.

4. The Integer Quantum Hall Effect

The integer quantum Hall effect (IQHE) was first observed in 1980 by v. Klitzing [2] in a Si-MOSFET (Metal-Oxide-Semiconductor Field Effect Transistor.) in an environment of low temperatures of the order $T \approx 0,3 K$.

It is worth to mention that MOSFET is a useful device that can generate electron concentrations ranging from $(0 - 10^{13}) cm^{-2}$ by varying the gate voltage [14].

According to the further developments, one can define a suitable temperature to be one such that $k_B T \ll \hbar\omega_B$, with the former denoting the thermal energy fluctuations while the latter is the Landau model quantum associated with the Hall effect.

The transverse resistance versus external magnetic field plot has plateaus at some fixed values

$$\rho_{xy} = \frac{h}{e^2\nu} \tag{7}$$

with ν belonging to the integer numbers.

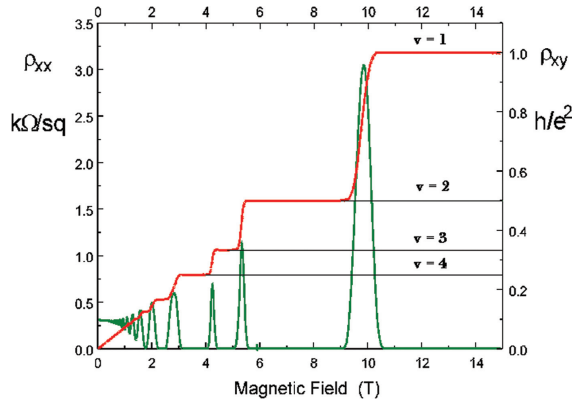


Figure 2: Typical measurement of the integer quantum Hall effect. The Hall resistivity exhibits plateaus. The longitudinal resistance (green) has a peak at every transition to the next plateau [25].

Its dependence on the external magnetic field is given in the Figure 2, with plateaus at some fixed quantized levels and peaks in the longitudinal resistance at the transition to the next plateau.

Since 1990, the (IQHE) quantum

$$R_K = \frac{h}{e^2} = 25812.807\Omega \quad (8)$$

is regarded as the resistance standard, with the subscript K being in honour of v.Klitzing [6]. This quantum is measured with very high precision of, at least, $1/10^{10}$.

4.1. The Integer Quantum Hall Effect: Landau Levels

The quantum Hall effect is observed in junctions such as the Si/SiO₂ in a MOSFET transistor or in GaAs/AlGaAs heterostructures, for example. The (IQHE) can also be verified in a wide range of systems like HgTe/CdTe, Si/Ge, etc. By applying an adequate gate voltage at these systems, electrons are trapped in a specific region with small width of 50 – 100 Angstroms, being nearly planar [14]. Therefore, the study of 2D electron gases is convenient to model both (IQHE) and (FQHE).

The integer quantum Hall effect is associated to the case of approximately non-interacting electrons. In order to describe it, the Lagrangian of a two-dimensional charged particle under an external magnetic field

$$L = \frac{m\dot{x}^2}{2} - e\dot{x}_i A^i(x) \quad (9)$$

must be considered.

The $A^i(x)$ field appearing above denotes the electromagnetic vector potential. The Landau gauge is considered $\vec{A} = xB\mathbf{e}_y$ with \mathbf{e}_y denoting the unit vector in the y direction. It means that the residual translation symmetry is associated to this coordinate.

The correspondent Hamiltonian reads

$$H = \frac{(p_i + eA_i)^2}{2m} \quad (10)$$

with $p_i = m\dot{x}_i - eA_i$.

Considering the well known fundamental Poisson Brackets from classical mechanics [26] and the correspondence principle², one gets

$$[\pi_x, \pi_y] = i\hbar B, \quad [a, a^\dagger] = 1 \quad (11)$$

with

$$\pi_i = m\dot{x}_i, \quad a = \frac{1}{\sqrt{2e\hbar B}}(\pi_x - i\pi_y) \quad (12)$$

The Problem reduces to the quantum harmonic oscillator algebra, see the introductory reference [27]. The Hamiltonian can be rewritten as

$$H = \frac{1}{2m}\pi_i\pi^i = \hbar\omega_B \left(a^\dagger a + \frac{1}{2} \right) \quad (13)$$

in, which ω_B denotes the cyclotron frequency.

The spin degree of freedom is not taken into account. Although in principle, the energy displacement due to the Zeeman effect seems to have the same value of the Landau level quanta, the former should be computed with regard to an effective mass due to interaction with the environment. Then, for GaAs system, the Landau quantum is 70× bigger than the one associated to the Zeeman effect [4]. The magnetic field is considered to be intense enough to polarize all the spins to minimize this interaction energy [6].

Beyond the creation/annihilation operator approach, it is instructive to evaluate the standard wave function analysis. Considering the chosen gauge, the translation invariance in \mathbf{e}_y motivates us to consider the following ansatz for the wave function

$$\psi_k(x, y) = e^{iky} f_k(x) \quad (14)$$

The solution has two labels defining the eigenstates of the Hamiltonian

$$\psi_{n,k}(x, y) \propto e^{iky} H_n(x + kl_B^2) \exp\left(-\frac{(x + kl_B^2)^2}{2l_B^2}\right) \quad (15)$$

here, n denotes the Landau level, k is a real number and $H_n(x)$ are the Hermite Polynomials. $l_B = \sqrt{\frac{\hbar}{eB}}$ is the so-called magnetic length. For $B \sim 1T$, $l_B \approx 2,5 \times 10^{-8} m$. The problem has a similarity with the familiar harmonic oscillator quantization.

The presence of the continuous k label implies in a large degeneracy for each Landau level

$$\mathcal{N} = eBA/h \quad (16)$$

² $i\hbar\{, \} \rightarrow [,]$

with A being the area of the planar sample and \mathcal{N} denoting the number of states with the same Landau level.

The quantum Hall effect phenomenology is achieved by introducing an electric field in the \mathbf{e}_x direction leading to a change in the Hamiltonian as $H \rightarrow H + eEx$.

The correspondent new eigenstates are

$$\psi(x, y) = \psi_{n,k} \left(x + \frac{mE}{eB^2}, y \right) \quad (17)$$

The energy now depends on this parameter k

$$E_{n,k} = \hbar\omega_B \left(n + \frac{1}{2} \right) - eE \left(kl_B^2 + \frac{eE}{m\omega_B^2} \right) + \frac{mE^2}{2B^2} \quad (18)$$

A group velocity in the y direction, related to the transverse current, arises

$$\mathcal{V}_y = \frac{1}{\hbar} \frac{\partial E_{n,k}}{\partial k} = -\frac{E}{B} \quad (19)$$

Now, before finishing this section, it is worth mentioning that the so-called symmetric gauge

$$2\vec{A} = \vec{r} \times \vec{B} = -yB\mathbf{e}_x + xB\mathbf{e}_y \quad (20)$$

is another legitimate choice which is particularly useful for discussing the fractional quantum Hall effect. This review is made in section 9.

It breaks the translational invariance, but the rotational one is kept. Defining the variable $z = x - iy$, the wave function reads

$$\psi_g(z, z^*) \sim \left(\frac{z}{l_B} \right)^g \exp[-z^*z/4l_B^2], \quad (21)$$

$$J_z \psi_g(z, z^*) = \hbar g \psi_m(z, z^*)$$

which is also an eigenstate of the z component of the angular momentum operator with eigenvalue g .

5. Quantized Conductivity

The transport properties of the system can be calculated in terms of the previously derived wave functions. Then, since the mechanical momentum reads $m\dot{x}_i = p_i + eA_i(x)$, the superficial current density is defined as $J_i = -\frac{e}{A}\dot{x}_i$, with the expectation value given below

$$\vec{J} = -\frac{e}{mA} \sum_n \sum_k \langle \psi_{n,k} | (-i\hbar\vec{\nabla} + e\vec{A}) | \psi_{n,k} \rangle \quad (22)$$

$$J_x = 0 \quad (23)$$

with the sum over k being related to the degeneracy of the system, n is associated to the filled Landau Levels and A denotes the area of the sample. Therefore, this sum is being taken to derive an expectation value over the full set of filled states.

An intuitive manner to understand this result is considering the fact that the last expression resembles the expectation value of the momentum in a harmonic oscillator, since $A_x(x) = 0$ in the Landau gauge. Regarding the induced current perpendicular to the applied electric field, associated to the Hall effect, it is calculated as

$$J_y = -\frac{e}{mA} \sum_n \sum_k \langle \psi_{n,k} | \left(-i\hbar \frac{\partial}{\partial y} + e x B \right) | \psi_{n,k} \rangle$$

$$= e\nu \sum_k \frac{E}{AB} \quad (24)$$

in which $\langle \psi_{n,k} | x | \psi_{n,k} \rangle = -\frac{\hbar k}{eB} - \frac{mE}{eB^2}$ and $-i\langle \psi_{n,k} | \frac{\partial}{\partial y} | \psi_{n,k} \rangle = k\langle \psi_{n,k} | | \psi_{n,k} \rangle$ as can be readily computed considering the previously obtained energy eigenstates.

The sum over k gives the degeneracy of the system $AB\frac{e}{h}$. The conductivity tensor is associated with the following expression

$$J_i = \sigma_{ij} E_j \quad (25)$$

with the sum over repeated indices, representing the matrix multiplication.

Then, one notices that only σ_{xy} is non-vanishing since

$$J_y = e^2 \nu \frac{E}{h} \quad (26)$$

and the electric field is placed along the x axis.

Then, in this specific case, the transverse resistivity is given by the inverse of σ_{xy}

$$\rho_{xy} = \frac{h}{e^2 \nu} \quad (27)$$

from which the quantized Hall resistivity can be inferred. Note that it reproduces the quantized resistivity depicted in Figure 2.

Considering the case of samples with boundaries under external magnetic field, the bulk electrons are confined in an area delimited by its cyclotron movement. However, at the boundary, there are extended states with non-vanishing drift velocity in the \mathbf{e}_y direction, see the Figure 3.

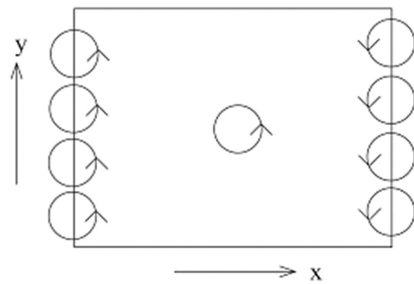


Figure 3: Due to the cyclotron movement, the conducting extended states that contribute to the electric current appears just at the boundary. Each one moves in opposite directions. The bulk states are localized [4].

6. Adding Impurity to the Sample

Interestingly, although clean samples are necessary if one wants to produce (QHE) phenomenon, a small amount of impurity is necessary for the formation of the plateaus.

This is due to the following. Considering a very clean sample, impurity may be modeled by a small perturbation. It can be described as a localized potential

$$|\vec{\nabla}V| \ll \frac{\hbar\omega_B}{l_B} \tag{28}$$

The density of states changes as in Figure 4. As it is going to be discussed in the next sections, the impurity generates localized bulk states around them. Differently from the extended states, these are non gaped accessible ones. Then, for a given Fermi energy, all the possible Landau levels are filled with just some remaining bulk local states to be occupied following the Pauli exclusion principle. Eventually, by rising this energy, the threshold for the next Landau level is achieved and part of the bulk states can occupy the extended boundary ones, see Figure 5.

Since the magnetic B field is intense, we focus on a situation with just an external magnetic field (perpendicular to the sample.) and the Lorentz force

$$x(t) = X - Rsen(\omega_B t + \phi), \quad y(t) = Y + Rcos(\omega_B t + \phi) \tag{29}$$

with the radius R, the phase ϕ and the guiding center (X,Y) being arbitrary.

In the presence of impurity, the Hamiltonian changes as $H \rightarrow H + V$. Since

$$X = x - \frac{\pi_y}{m\omega_B}, \quad Y = y + \frac{\pi_x}{m\omega_B}, \tag{30}$$

one gets

$$\begin{aligned} i\hbar\dot{X} &= [X, H + V] = il_B^2 \frac{\partial V}{\partial Y}, \\ i\hbar\dot{Y} &= [Y, H + V] = -il_B^2 \frac{\partial V}{\partial X} \end{aligned} \tag{31}$$

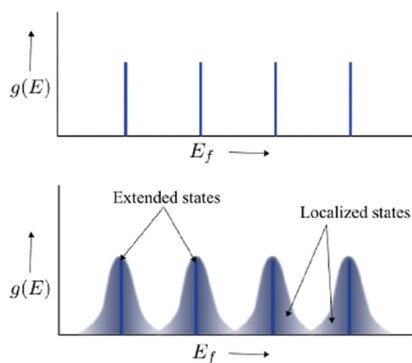


Figure 4: The inclusion of the impurity defines a continuous spectrum of energy, instead of just the discrete Landau levels [6]. It allows the existence of accessible continuous states in the bulk. The extended states are gapped and observed just after reaching the threshold energy associated to the discrete Landau levels.

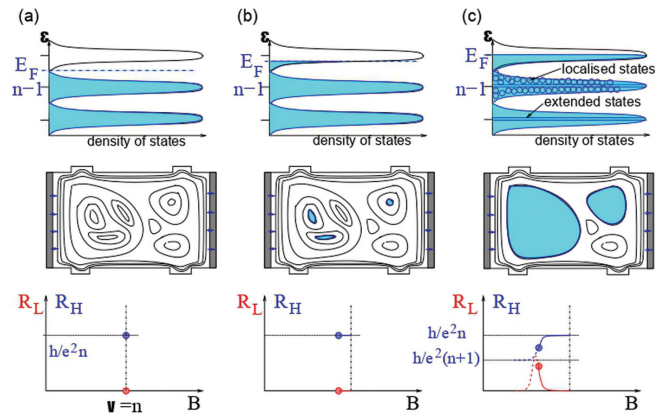


Figure 5: Equipotential lines, occupied states and transverse (blue)/longitudinal (red) resistance behaviour [6]. There is a peak in the longitudinal resistance R_L when the threshold energy of the next (LL) level is achieved. At this moment the Hall resistance falls since the next Landau level is filled. Then, R_H goes to the next plateau.

Therefore, the guiding center drift along equipotential, $\dot{\vec{R}}$ is perpendicular to $\vec{\nabla}V$.

6.1. Localized and Extended States

As discussed, the localized states are the bulk ones and the extended states are on the boundary. According to Figure 4, since the Landau Levels (LL) are gaped, by increasing the energy, the electrons start to populate the bulk energy levels. Due to the fermionic nature, these particles cannot occupy the same state. Therefore, when the energy reaches the threshold value, the electrons start to fill the next (LL) and the transverse current increases [5, 6]. It explains the formation of plateaus as due to the invariance of the transport properties under small variations of the system's parameters.

A similar idea explains the plateau formation in transverse resistivity depicted in the Figure 2. With an increasing magnetic field, the degeneracy as well as the distance between two consecutive Landau levels increase. Then, when a given previously filled level becomes bigger than the Fermi energy, the electrons start to scatter due to the increase of the degeneracy. The filling factor decreases and the transverse resistivity goes to the next plateau. In this transition, both the longitudinal current and the longitudinal resistance have a peak, since the latter is related to the former as $\rho_{xx} = \sigma_{xx} / (\sigma_{xx}^2 + \sigma_{xy}^2)$. This is due to the fact that increasing the degeneracy of Landau levels, some previously localized bulk states become capable to occupy the extended boundary ones.

Summing up, after the lower energy level is filled, the electrons have nowhere to scatter and the longitudinal resistance falls back to zero again. One can also note that the bigger the magnetic field is, the bigger the amplitude

of the peak becomes, since the degeneracy increases and there are more states for the electrons to scatter into.

6.2. On the Topological Nature of the Quantum Hall Effect

The quantum Hall effect is a robust phenomenon which is resistant under small variations of the material's parameters. It also has the universality property; very low dependence on the specific structure of the matter samples included in the class of materials in which it can be realized. For example, the Hall transport properties on the Si-MOSFET are the same as in the GaAs one up to an uncertainty of $\approx 4 \times 10^{-10}$! It indicates that there must be a more fundamental reason for this feature. Here, a brief discussion about the topological nature of this effect is provided.

In a crystal structure, the momenta are confined on a torus T^2 with $-\pi/a < k_x < \pi/a$ and $-\pi/b < k_y < \pi/b$ with a being the distance between two consecutive sites in the \mathbf{e}_x direction and b the distance between two sites in the \mathbf{e}_y direction. Obviously, this is the correct description just for a specific kind of lattice. However, since this torus structure is present for planar lattices and the interest is on the topological properties, this discussion can be relevant for the general case. In order to describe the topological aspects of the (QHE), the only necessary conditions are a system whose spectrum decomposes into bands [4], approximately non-interacting electrons, and the fact that there is a gap between the bands with the Fermi energy staying between them.

From the system's eigenstates, one gets the Berry connection [28] associated to adiabatic variations of the momentum labels

$$\mathcal{A}_i(k) = -i \langle u_k(x) | \frac{\partial}{\partial k^i} | u_k(x) \rangle \quad (32)$$

with $|u_k(x)\rangle$ associated to Bloch states $|u_k(\vec{x})\rangle = |u_k(\vec{x} + \vec{G})\rangle$ for $G = (0, a)$ or $G = (0, b)$.

The curvature $\mathcal{F}_{xy}(k) = \frac{\partial}{\partial k_x} \mathcal{A}_y(k) - \frac{\partial}{\partial k_y} \mathcal{A}_x(k)$ is used to construct the T.K.N.N topological invariant³, which is related to the conductance as

$$C = -\frac{1}{2\pi} \int_{T^2} d^2k \mathcal{F}_{xy}(k), \quad \sigma_{xy} = \frac{e^2}{2\pi\hbar} \sum_{\alpha} C_{\alpha} \quad (33)$$

The C_{α} denotes the topological invariant associated to each filled band. It is valued on the natural numbers, see [14] for detailed derivation from the Kubo formula. It is robust against small variation of the system's parameters, showing that the (QHE) phenomenology has indeed a topological nature [29]. It is a deeper explanation for the universality of such effect. It can be observed in a class of samples such as semiconductors and also graphene-like systems with honeycomb lattice. It is worth to mention that this number is non-vanishing just

for discrete symmetry breaking systems. For example, in the presence of an external magnetic field. However, in this case, the definition of the Bloch states becomes more subtle.

7. Fractional Quantum Hall Effect

In 1982 some quantum Hall systems [3], were discovered with fractional filling fractions ν with $\nu = 1/3$. Latter, several fractional values, such as, $\nu = 2/5, 3/7, \dots$ were also observed. These are semi-filled Landau levels (LL). As an example of a system in which it can occur, one can mention GaAs/AlGaAs heterostructures furnishing high quality 2D electron gases with high mobility [6]. For the case of GaAs structures, the range of concentrations is $(10^{11} - 10^{12}) \text{cm}^{-2}$.

Fractional Hall conductivities can also be realized in high mobility MOSFET. The temperature of the original measurements was of order $T \approx 0,48$ K. The plateaus are less prominent in this case. This is due to the fact that the samples are of high mobility, being associated to low presence of impurities.

The (FQHE) is generally observed for external magnetic fields on the range $B \geq 10$ T [14]. The filling fractions are obtained with an experimental precision of, at least, $\approx 3/10^5$.

The semi-filled levels present high degeneracy. By changing the system's parameters, the electrons can scatter into other states at the same Landau-Level. Then, in order to describe this system, the interactions between electrons in a given (LL) must be taken into account.

It is an interacting system with a huge number of particles due to the large degeneracy. An exact answer is extremely difficult, so one must use an approximation method.

As mentioned, this phenomenon has less dependence on the impurities. Namely, it is characterized by the following hierarchy of interaction scales

$$\hbar\omega_B \gg E_{Coulomb} \gg V_{impurity} \quad (34)$$

This is a consequence of the fact that the effective mass m^* of the charge carriers is smaller than the bare electron one. For example, it reads $m^* = 0,067m_e$ for the case of GaAs with m_e denoting the electron mass.

The Coulomb interaction is of the form

$$V(|\vec{r}_1 - \vec{r}_2|) \quad (35)$$

depending just on the radial distance of the particles. It implies that the angular momentum is conserved. Then, as previously mentioned, it is convenient to work in the symmetric gauge on a wave function for many particles which is also an eigenstate of angular momentum, the Laughlin wave function [15]

$$\psi(z_1, \dots, z_n) = \prod_{i < j}^N (z_i - z_j)^g \exp \left(- \sum_{i=1}^N |z_i|^2 / 4l_B^2 \right) \quad (36)$$

³ In honor of Thouless, Kohomoto, Nightingale and Nijs.

with g being an odd integer in order to respect the fermionic nature under exchange of z_i and z_j coordinates. Π denotes a productory and N is the number of particles.

7.1. The Filling Factor

This section is devoted to verify that the Laughlin wave function indeed leads to the right filling fraction. Focusing on the particle 1, the Laughlin wave function gives $g(N - 1)$ as the maximum exponent of the particle coordinate z_1 . Therefore, we can show that

$$J_{max.} \approx g(N - 1)\hbar \tag{37}$$

Treating the particle 1 approximately as a free one, it is possible to show that its wave function has support on an area of radius $R = \sqrt{2gN}l_B$. Then, the area is

$$A \approx 2\pi gNl_B^2 \tag{38}$$

Since the degeneracy is $\mathcal{N} = eBA/h = gN$, the number of particles over the degeneracy gives the filling factor

$$\nu = \frac{1}{g} \tag{39}$$

with the desired fractional values.

The charge carriers are accommodated to minimize the Coulomb interaction, generating a realization of the Wigner crystal [6].

8. The Sample: The Graphene Description

After analyzing the general aspects of the phenomenon, the next step is the investigation of the specific content of a given matter sample. Regarding this specific example, it presents the so-called relativistic Landau levels when in the presence of a magnetic field. It is a generalization of the previously discussed non-relativistic case.

The graphene is a two-dimensional material composed by carbon atoms. Namely, the valence electrons are disposed in a sp^2 hybridization and the remaining one is in an p_z orbital [17]. The former electrons form sigma bonds with the sp^2 ones of the neighboring atoms. The electrons in the p_z orbitals do not enter these bonds. The sp^2 orbitals are in the same plane and form angles of 120° between them [18, 19]. Novoselov and Geim [30] won the Nobel Prize in 2010 due to previous experimental works related to graphene planar material. It has the lattice structure of the Figure 6.

Remarkably, there are two different kinds of elements in this honeycomb lattice. The A and B sites have different crystallographic classifications since their lattice neighborhoods are different [17, 18]. This lattice is

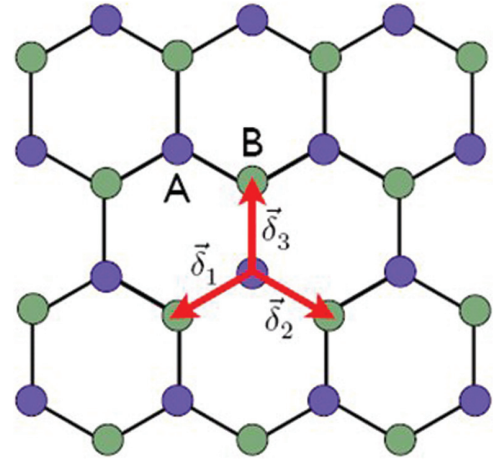


Figure 6: Lattice structure of graphene [31].

defined by the vector basis

$$\begin{aligned} \delta_3 &= \frac{a}{\sqrt{3}}\mathbf{e}_y, & \delta_1 &= -\frac{a}{\sqrt{3}}\left(\frac{\sqrt{3}}{2}\mathbf{e}_x + \frac{1}{2}\mathbf{e}_y\right) \\ \text{and } \delta_2 &= \frac{a}{\sqrt{3}}\left(\frac{\sqrt{3}}{2}\mathbf{e}_x - \frac{1}{2}\mathbf{e}_y\right) \end{aligned} \tag{40}$$

with $\frac{a}{\sqrt{3}} = 0,142 \text{ nm}$, which connects one basis element to its first neighbors.

The Hamiltonian proposed by Philip R. Wallace in 1947 to model the band structure of monolayer graphite (graphene) [32] presents a tight binding structure in which the p_z electrons are governed by the Hamiltonian

$$H = -t \sum_{R;i=1,2,3;\sigma=\pm} (C_B^\dagger(R + \delta_i, \sigma)C_A(R, \sigma) + H.C.) \tag{41}$$

in which the coupling t is of order 3 eV, σ denotes the spin orientations and $C_B^\dagger(R + \delta_i, \sigma)$ is a creation operator of an p_z electron with spin σ located in $(R + \delta_i)$.

Using the Fourier transform

$$C_{A,B}(r, \sigma) = \frac{1}{N} \sum_k C_{A,B}(k, \sigma)e^{ik \cdot r} \tag{42}$$

the Hamiltonian can be rewritten as

$$\begin{aligned} H &= \sum_{k,\sigma} (-tC_A(k, \sigma)C_B^\dagger(k, \sigma) \sum_i e^{ik \cdot \delta_i} + H.C.) \\ &= \sum_{k,\sigma} \psi^\dagger(k, \sigma) \begin{pmatrix} 0 & \phi \\ \phi^* & 0 \end{pmatrix} \psi(k, \sigma) \end{aligned} \tag{43}$$

with $\phi(k) = -t \sum_l e^{ik \cdot \delta_l}$ and $\psi^\dagger(k, \sigma) \equiv (C_A^\dagger(k, \sigma), C_B^\dagger(k, \sigma))$.

The energy eigenvalues define the two band structure

$$E(k) = \pm|\phi(k)| = \pm \sqrt{\sum_{l,j} e^{ik \cdot (\delta_l - \delta_j)}} \tag{44}$$

There are two points in the reciprocal lattice for which the valence and the conduction bands have a zero energy gap between them. These points are located at the Brillouin zone corners $K_{\pm} = \pm \frac{4\pi e_x}{3a}$ leading to $\phi(K_+) = \phi(K_-) = 1 + e^{i\frac{2\pi}{3}} + e^{-i\frac{2\pi}{3}} = 0$.

A low energy Hamiltonian can be obtained considering the expansion near the Dirac points $K = K_{\pm} + p$ which, after the canonical transformation $\psi_{K_{\pm}}(k, \sigma) \rightarrow e^{i\frac{\sigma z \pi}{2}} \sigma_x \psi_{K_{\pm}}(k, \sigma)$, assumes the form

$$H_{K_+} = \psi_{K_+}^\dagger(k, \sigma) h_{K_+} \psi_{K_+}(k, \sigma) \tag{45}$$

$$H_{K_-} = \psi_{K_-}^\dagger(k, \sigma) h_{K_-} \psi_{K_-}(k, \sigma) \tag{46}$$

in which $h_{K_+} = h_{K_-} = v(p_x \sigma_x + p_y \sigma_y) + \mathcal{O}(p^2)$ and the effective velocity $v_F = \frac{\sqrt{3}ta}{2}$ depends on the microscopic details of the lattice. It is a relativistic velocity since it is comparable to the light velocity

$$v \sim \frac{c}{300} \tag{47}$$

The energy eigenvalues are $E(\vec{k}) = \pm v|\vec{k}|$. The two solutions for the low energy Hamiltonian are the so-called Dirac valleys.

The graphene is a kind of material with promising applications in technology due to its unusual properties. The quasi-particles of this system must be treated as relativistic ones with a vanishing effective mass. The effective Hamiltonian of the model under an external magnetic field is obtained by the use of the minimal coupling procedure (in the Landau Gauge) and leads to the structure below in which a specific valley is analyzed [6]

$$H = v(\vec{p} + e\vec{A}) \cdot \vec{\sigma} \tag{48}$$

Explicitly, it reads

$$H = v \begin{pmatrix} 0 & \pi_x - i\pi_y \\ \pi_x + i\pi_y & 0 \end{pmatrix} = \sqrt{2} \frac{\hbar v}{l_B} \begin{pmatrix} 0 & a \\ a^\dagger & 0 \end{pmatrix} \tag{49}$$

with v_F denoting the drift velocity in graphene and a and a^\dagger are the creation and annihilation operators previously defined in the Landau problem analysis. The relativistic Landau levels are

$$E_n = \lambda \sqrt{2n} \left(\frac{\hbar v_F}{l_B} \right) \tag{50}$$

with $\lambda = \pm$. The sign $+$ is related to the conduction band and $-$ to the valence band. Here, n are natural numbers and denote the Landau levels. It has square root dispersion instead of a linear one like in the non-relativistic case, see Figure 7.

Regarding the empirical observation of relativistic Landau levels, the associated signatures have been experimentally inferred in transmission spectroscopy by sending photons to the sample and measuring the intensity of the transmitted light. The experiments have been

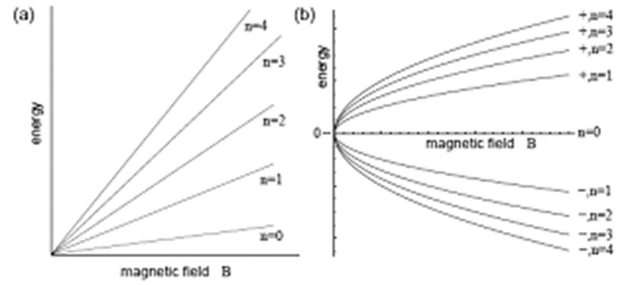


Figure 7: Comparison between non-relativistic (a) and relativistic (b) energy states dependence with the external magnetic field [6].

performed on the epitaxial graphene [33] and later on exfoliated graphene [34]. When the monochromatic light is in resonance with a dipole-allowed transition from the (partially) filled LL ($\pm n$) to the (partially) unoccupied LL ($\pm, n \pm 1$), the light is absorbed due to an electronic excitation between the two levels. The possible allowed transitions are

$$\Delta_{n,\epsilon} = \frac{\hbar v}{l_B} \left[\sqrt{2n+1} - \epsilon \sqrt{2n} \right] \tag{51}$$

$\epsilon = +$ denotes transition in the same band and $\epsilon = -$ between different ones.

This is the observable output of the theory and indeed provides an accurate description of the phenomenology.

The relativistic Landau levels receive this name due to the similarity between the low energy description of the associated graphene layer and the one of a massless relativistic fermionic particle. However, since v is different from the light velocity, the system indeed violates Lorentz symmetry, despite the mentioned analogy. In this case, not just the Landau levels change their structure, but also the Hall resistivity. It can be proved that the Hall resistance $R_H = \frac{h}{e^2 \nu}$ is associated to the following filling fractions [18]

$$\nu = 2(2n + 1) \tag{52}$$

which are restricted to the values $\nu = \pm 2, \pm 6, \pm 10, \dots$. The overall factor 2 is associated with the spin degeneracy. It is worth mentioning that this is a representative of the integer quantum Hall effect.

9. Effective Field Description: FQHE

for $\nu = \frac{1}{2k+1}$

Throughout this section, we provide a detailed review of the approach of [16] for planar electrons on a perpendicular magnetic field, interacting by means of a scalar Coulomb potential. It is proved that there exists a canonical transformation relating this system to another one with bosonic, instead of fermionic, matter particles with attached magnetic flux. There is also the addition of the so-called statistical field to induce this

magnetic flux. Due to the Aharonov-Bohm effect, see the introductory review on the reality of the physical potentials [35], these bosons behave as fermions under particle exchange. Moreover, the mentioned canonical transformation exists just for a set of quantized values for the statistical field normalization. Then, after computing the transport properties of the system, it is possible to verify a quantized transverse conductance characteristic of the fractional quantum Hall effect.

The Hamiltonian for a two-dimensional sample with a macroscopic number of electrons under a perpendicular magnetic field and a scalar potential, reads

$$H = \frac{1}{2m} \sum_i [\vec{p}_i - e\vec{A}(x_i)]^2 + \sum_i eA_0(x_i) + \sum_{i<j} V(x_i - x_j) \tag{53}$$

The symmetric gauge $2A_i = B\epsilon_{ij}x_j$ is considered here. The Coulomb interaction between electrons is

$$V(|\vec{x}_i - \vec{x}_j|) = -\frac{e^2}{4\pi\epsilon_0|\vec{x}_i - \vec{x}_j|} \tag{54}$$

The eigenvalue problem is defined as $H\psi(x_1, \dots, x_n) = E\psi(x_1, \dots, x_n)$. The wave function $\psi(x_1, \dots, x_n)$ is antisymmetric under exchange of \vec{x}_i and \vec{x}_j coordinates, due to the fermionic nature. We do not take into account the spin, since a magnetic field strong enough to polarize the electrons is considered.

This Hamiltonian can be related by a unitary transformation to

$$H = \frac{1}{2m} \sum_i [\vec{p}_i - e(\vec{A}(x_i) + \vec{a}(x_i))]^2 + \sum_i eA_0(x_i) + \sum_{i<j} V(x_i - x_j) \tag{55}$$

in which

$$\vec{a}(x_i) = \frac{\hbar\theta}{e\pi} \sum_{j \neq i} \vec{\nabla} \alpha_{ij} \tag{56}$$

and $H\phi(x_1, \dots, x_n) = E\phi(x_1, \dots, x_n)$. The system has the same eigenvalues as before, but $\phi(x_1, \dots, x_n)$ is now symmetric under particle exchange, it is bosonic! α_{ij} is the angle between the particle i and the particle j with relation to the \mathbf{e}_x axis.

It is possible to show that just for the values $\theta = (2k + 1)\pi$, with k being a natural number, there is a unitary transformation

$$\mathbf{U} = \exp \left[-i \left(\frac{\theta}{\pi} \sum_{j>i} \alpha_{ij} \right) \right] \tag{57}$$

with $\psi(x_1, \dots, x_n) = \mathbf{U}\phi(x_1, \dots, x_n)$

$$\mathbf{U}[\vec{p}_i - e(\vec{A}(x_i) + \vec{a}(x_i))]\mathbf{U}^{-1} = \vec{p}_i - e\vec{A}(x_i) \tag{58}$$

The Hamiltonian can be expressed in terms of the density functional

$$H_1 = \int d^2x \phi^\dagger \left(\frac{1}{2m} [\vec{\nabla} - e(\vec{A}(x) + \vec{a}(x))]^2 + eA_0(x) \right) \phi + \frac{1}{2} \int d^2x d^2y \delta\rho(x)V(x-y)\delta\rho(y) \tag{59}$$

the fluctuation is defined as $\delta\rho(x) = \rho(x) - \mathcal{P}$. Here, $\rho(x) = \phi^\dagger(x)\phi(x)$ is the density operator and \mathcal{P} denotes its average value.

Considering a continuous notation, we have the definition of the so-called statistical Chern-Simons field

$$a^i(x) = -\frac{\hbar\theta}{e\pi} \epsilon^{ij} \int d^2y \frac{x^j - y^j}{|x^j - y^j|} \rho(y) \tag{60}$$

The Lagrangian associated to the new vector field equations of motion is the Chern-Simons one which is a topological invariant. It is given below

$$\mathcal{L}_2 = \frac{e^2\pi}{2\theta\hbar} \epsilon^{\nu\alpha\beta} a_\nu \partial_\alpha a_\beta - a_\mu J^\mu \tag{61}$$

It is invariant under $a_\mu(x) \rightarrow a_\mu(x) + \partial_\mu\Lambda(x)$ up to a boundary term. The $a_0(x)$ component can be understood as a Lagrange multiplier.

The equations of motion, in the case of the mean field solution $\vec{a}(x) = -\vec{A}(x)$, express the quantized Hall conductivity and the fact that a magnetic flux is attached to the charge carriers

$$e\rho(x) = \mathcal{K}B(x) \tag{62}$$

$$J^i(x) = \mathcal{K}\epsilon^{ij}E_j(x) \tag{63}$$

with $\mathcal{K} = \frac{e^2}{h(2k+1)}$.

The expressions above describe the expected phenomenology of the Hall effect for a class of fractionally quantized conductivities.

The circulation of the statistical gauge field is

$$\oint \vec{a} \cdot d\vec{l} = (2k + 1) \frac{h}{e} \tag{64}$$

using that $\int d^2y \rho(y) = 1$.

Therefore, since the Chern-Simons field attaches a magnetic flux on the matter particles, these particles receive an Aharonov-Bohm phase due to their exchange which is equal to

$$\exp \left(i \frac{e}{h} \int_0^\pi \vec{a} \cdot d\vec{l} \right) = -1 \tag{65}$$

This extra phase can be interpreted as a statistical changing from fermions to bosons and vice-versa. It is another confirmation of the fact that the unitary transformation can relate field descriptions with different associated statistics.

The Lagrangian associated to the scalar field part reads

$$\begin{aligned} \mathcal{L}_\phi &= \phi^\dagger (i\hbar\partial_t - e(A_0 + a_0))\phi \\ &- \phi^\dagger \left(\frac{1}{2m} [\vec{\nabla} - e(\vec{A}(x) + \vec{a}(x))]^2 + eA_0(x) \right) \phi \\ &- \frac{1}{2} \int d^2y \delta\rho(x)V(x-y)\delta\rho(y) \end{aligned} \quad (66)$$

9.1. Vortex Solution

Now, another solution for the bosonic scalar field is considered, a vortex one. The vortex solution is found by imposing non-trivial conditions on these fields at the spatial infinite. Although a neutral vortex need infinite energy, a charged one requires just a finite amount. The asymptotic configuration at $|\vec{x}| \rightarrow \infty$ is

$$a_0 = 0, \quad \phi = \sqrt{\mathcal{P}}e^{\pm i\alpha(x)}, \quad \delta\vec{a} = \pm \frac{\hbar}{e}\vec{\nabla}\alpha(x) \quad (67)$$

In this kind of solution there is a functional of the exponent of the asymptotic scalar field called winding number. It is related to the number of times the system gives a complete rotation in the internal field space when a complete rotation is performed in the real two-dimensional space. This number is a topological invariant and separates the space of solutions into disjoint classes. In this specific case, $\alpha(x)$ has a $\pm 2\pi$ displacement after a rotation around the origin.

This solution has finite energy since for $|\vec{x}| \rightarrow \infty$

$$\left(\frac{\hbar}{i}\vec{\nabla} - e\delta\vec{a}(x) \right) \phi(x) \rightarrow 0 \quad (68)$$

with the gauge field approaching something analogous to a pure gauge configuration⁴ at the spatial infinite. The charged vortex solution is conceived with a particular structure to ensure a finite energy. Then, the asymptotic gauge field is dependent from the exponent of the asymptotic scalar field.

Therefore, considering the properties of this solution, one can derive

$$\oint \delta\vec{a}\cdot d\vec{l} = \pm \frac{h}{e} \quad (69)$$

with the integral being performed in the line that delimits the region where the vortex solution occur.

The charge density related to a given gauge field configuration is given by the following equation of motion

$$\tilde{\rho}(x) = -\frac{\partial S}{\partial a_0(x)} = \frac{e^2}{h}\nu\epsilon^{ij}\partial_i a_j(x) \quad (70)$$

⁴ It has just an analogous form but is not equal since α behaves as a polar angle and then the derivatives applied on this function do not commute since it is not well-defined when the radial coordinate is zero. Therefore, it is not a symmetry of the model, the Chern-Simons strength tensor does not vanish in this configuration.

with $\tilde{\rho}(x)$ representing the charge density and S representing the action associated to the investigated Lagrangian.

Therefore, the vortex charge can be calculated [16] considering the specific gauge field solution for this case

$$Q = \int d^2x \tilde{\rho}(x) = \pm \frac{e}{2k+1} \quad (71)$$

leading to excitations with fractional charges.

10. Conclusions and Perspectives

The quantum Hall effect is a robust phenomenon of topological character that depends just on the long distance behavior of the sample, leading to an independence of its specific microscopic structure. The quantized conductivity has a topological nature, being related to the so-called T.K.N.N invariant.

For the case of the fractional quantum Hall effect, we investigated the unitary transformation that maps a fermionic system into a bosonic one if a given set of fractional values are admitted for the conductivity. The Chern-Simons excitation arises in this context as the statistical field that attaches a magnetic flux on the scalar particles, turning them into fermions by means of the Aharonov-Bohm effect.

The lattice structure of the graphene, one of the planar materials that can present the quantum Hall effect, was studied in the paper and its low energy excitations were carefully obtained.

As a future perspective, we intend to explore field descriptions of two and three-dimensional topological insulators [19] since the phenomenology can be visualized as two opposite Hall currents, without the need of an external magnetic field. Its role is played by the spin-orbit effect. Occurring at the boundary, each of these currents is correlated to a specific unique definite spin configuration, the so-called helical states, leading to no overall charge current.

Acknowledgements

G.B. de Gracia thanks FAPESP Post Doctoral grant No. 2021/12126-5 for financial support and B.M. Pimentel thanks CNPq for partial support.

References

- [1] E.H. Hall, American Journal of Mathematics **2**, 3, pp. 287–292 (1879).
- [2] K.v. Klitzing, G. Dorda, and M. Pepper, Phys. Rev. Lett. **45**, 494, (1980).
- [3] D.C. Tsui, H.L. Stormer, and A.C. Gossard, Phys. Rev. Lett. **48**, 1559, (1982).
- [4] D. Tong, *Lectures on Quantum Hall Effect*, arXiv:1606.06687, (2016).

- [5] G.V. Dunne, *Aspects of Chern-Simons Theories*, 1998 Les Houches Summer School. arXiv: hep-th/9902115, (1999).
- [6] M.O. Goerbig, *Quantum Hall Effects*. arXiv:0909.1998, (2009).
- [7] K.S. Novoselov, Z. Jiang, Y. Zhang, S.V. Morozov, H.L. Stormer, U. Zeitler, J.C. Maan, G.S. Boebinger, P. Kim, A.K. Geim, *Science* (2007), **315**, 1379–1379.
- [8] E. Ramsden, *Hall-effect sensors: theory and applications* (2 ed.). Elsevier. ISBN 978-0-7506-7934-3 (2006).
- [9] R.S. Popović, *Hall effect devices* (2 ed.). CRC Press. ISBN 978-0-7503-0855-7 (2004).
- [10] D. Baccino, S.L. Falcón and G.P. Trinidad, *Rev. Bras. Ensino Fís.*, **40**, 4, e4309 (2018).
- [11] C.E. Armentrout, *Amer. J. of Phys.* **58**, 758 (1990).
- [12] A.A. Soares, J.B.P. Junior, A.P.F. Moreira and L.C. Chiavini, *Rev. Bras. Ensino Fís.* **43** e20210185 (2021).
- [13] F.B. Kneubil and R. Karam, *Rev. Bras. Ensino Fís.* **39**, 2, e2302, (2017).
- [14] T. Chakraborty and P. Pietilainen, *The quantum Hall Effects, Integer and Fractional*, 2nd Elarged and Updated edition, Springer Series in Solid-State Sciences, vol. 85 (1995).
- [15] R.B. Laughlin, *Phys. Rev. Lett.* **50**, 1395 (1983).
- [16] S. Zhang, *Int. J. Mod. Phys. B*, **06**, 1, pp. 25–58, (1992).
- [17] E.C. Marino, L.O. Nascimento, V.S. Alves, C.M. Smith, *Phys. Rev. X* **5**, 1, 011040 (2015).
- [18] E.C. Marino, *Quantum Field Theory Approach to Condensed Matter Physics*, Cambridge University Press, (2017).
- [19] S.Q. Shen, *Topological Insulators; Dirac equation in condensed matter.*, Springer-Verlag, Berlin, (2012).
- [20] Z. Jiang, Y. Zhang, Y.W. Tan, H.L. Stormer, P. Kim. *Solid state communications* **143**, (1–2), 14–19, (2007).
- [21] G. Pacchioni, *Nat. Rev. Mat.* **5**, 7, 480 (2020).
- [22] Zurich Instruments AG. *Using the Hall Effect for Nano Electronics*. AZoNano. 27 March 2023. <https://www.azonano.com/article.aspx?ArticleID=5177>
- [23] B.T. Schaefer, L. Wang, A. Jarjour et al. *Nat Commun* **11**, 4163 (2020).
- [24] N. Ashcroft and D. Mermin, *Solid State Physics*, Saunders College Publishing, 1st edition, (1976).
- [25] T. Kramer, *Rev. Mex. Fis. S* **52** (4), 49–55, (2006).
- [26] P.A.M. Dirac, *Lectures on Quantum Mechanics*, New York: Yeshiva University (1964).
- [27] D. Griffiths, *Introduction to Quantum Mechanics*, 2nd edition, Pearson Prentice Hall, (2004)
- [28] M.V. Berry, *R. Soc. Lond. A* **392** 45–57 (1984).
- [29] D.J. Thouless, M. Kohmoto, M.P. Nightingale, M. den Nijs *Phys. Rev. Lett.* **49** (6), 405 (1982).
- [30] A. Geim and K. Novoselov, *Nat. Phys.* **6**, 836 (2010).
- [31] F. de J. Sanz, *The influence of the morphology and long range interactions on the electronic properties of graphene*, [doctoral thesis, Autonomous University of Madrid] (2010). <https://repositorio.uam.es>
- [32] P.R. Wallace, *Phys. Rev.* **71**, 622 (1947).
- [33] M.L. Sadowski, G. Martinez, M. Potenski, C. Berger, W.A. de Heer, *Phys. Rev. Lett.* **97**, 266405 (2006).
- [34] Z. Jiang, E.A. Henriksen, L.C. Tung, Y-J Wang, M.E. Schwarz, M.Y. Han, P. Kim, H.L. Stormer, *Phys. Rev. Lett.* **98**, 197403 (2007).
- [35] G.L. Ferreira, *Rev. Bras. Ensino Fís.* **26**, 1, 27–31, (2004).